En Face Optical Coherence Tomography Imaging of Foveal Dots in Eyes With Posterior Vitreous Detachment or Internal Limiting Membrane Peeling

Cameron Pole,[1] Adrian Au,[1] Eduardo Navajas,[2] K. Bailey Freund,[3,4] Srinivas Sadda,[5,6] and David Sarraf[1,7]

[1]Retinal Disorders and Ophthalmic Genetics, Stein Eye Institute, University of California at Los Angeles, Los Angeles, California, United States
[2]Department of Ophthalmology and Visual Sciences, Eye Care Center, University of British Columbia, British Columbia, Vancouver, Canada
[3]Vitreous Retina Macula Consultants of New York, New York, New York, United States
[4]Department of Ophthalmology, New York University Grossman School of Medicine, New York, New York, United States
[5]Doheny Eye Institute, Los Angeles, California, United States
[6]University of California at Los Angeles, Los Angeles, California, United States
[7]Greater Los Angeles VA Healthcare Center, Los Angeles, California, United States

Correspondence: David Sarraf, Stein Eye Institute, University of California, Los Angeles, 100 Stein Plaza, Los Angeles, 90095 CA, USA; dsarraf@ucla.edu, sarraf@jsei.ucla.edu.

Received: December 19, 2020
Accepted: June 27, 2021
Published: August 5, 2021

Citation: Pole C, Au A, Navajas E, Freund KB, Sadda S, Sarraf D. En face optical coherence tomography imaging of foveal dots in eyes with posterior vitreous detachment or internal limiting membrane peeling. *Invest Ophthalmol Vis Sci.* 2021;62(10):5. https://doi.org/10.1167/iovs.62.10.5

Purpose. To analyze the morphology of foveal hyperreflective dots (HRD) identified with en face optical coherence tomography (OCT) and evaluate the effects of internal limiting membrane (ILM) peeling and posterior vitreous detachment (PVD) on the number of these lesions.

Methods. Retrospective cross-sectional study of patients with OCT angiography and en face OCT. Using en face OCT, superficial HRD lying on the foveal floor were measured and quantitated in eyes with ILM peel and in the fellow nonsurgical eyes. Eyes with foveal PVD were also compared to fellow eyes without foveal PVD. High-magnification en face OCT was also performed to better understand the morphology of HRD in the fovea.

Results. Eyes that underwent ILM peel (n = 10) displayed fewer HRD ($P = 0.012$) compared to control fellow nonoperated eyes. In eyes with foveal PVD, the mean number of HRD was numerically greater, but without statistical significance, compared to the contralateral eye without foveal PVD. High-magnification en face OCT illustrated HRD with irregular shapes and fine cilia-like or dendriform extensions. Average length of HRD was between 15 to 21 µm in all four groups.

Conclusions. HRD decreased in eyes with ILM peeling by en face OCT compared with fellow nonoperated eyes and exhibited a glial cell-like morphology and size closely resembling the white dot fovea described previously using scanning electron microscopy. HRD may represent processes of activated retinal glia, possibly Muller cells, that traverse defects in the ILM.

Keywords: hyperreflective dots, en face OCT, ILM peel, PVD

In a seminal study using scanning electron microscopy (SEM), Yokotsuka et al.[1] described the white dot fovea comprised of polygonal lesions with ciliary or dendritic-like processes in the central fovea. These findings were attributed to activated glial or Muller cell processes breaking through a thin internal limiting membrane as a result of chronic or increased vitreoretinal traction.

Optical coherence tomography (OCT) has revolutionized our understanding of macular diseases and therapeutic outcomes.[2] The newest spectral-domain and swept-source technologies can generate cross-sectional images of retinal anatomy that approximate histological specimens.[3] Additionally, high-density volumetric OCT scanning has enabled digital reconstruction of retinal layers in the coronal or en face plane, facilitating layer-by-layer analysis of the retina.[4,5] Several studies combining en face imaging and B-scan OCT have successfully analyzed retinal pathologies of both the inner[6,7] and outer[8,9] retinal layers.

Recently, Corradetti et al.[5] described the presence of superficial hyperreflective dots (HRD) on the surface of the fovea in a cohort of normal eyes using en face and B-scan OCT. These dots were quantified using a novel and validated algorithm, and the authors noted a systematic increase in the number of dots in normal eyes according to decade of age, especially over the age of 50. We believe that these HRD may represent the OCT signature of white dot fovea described by Yokotsuka et al.[1] with SEM. As posterior vitreous detachment (PVD) and ILM peeling can mechanically alter the surface of the fovea, we aimed to analyze the effects of these events on the presence, number, and area of HRD

Table 1. Comparison of Hyperreflective Dots Between Eyes With PVD and Fellow Eyes Without PVD

		***P* Values**
PVD Comparison		
Mean age (years)	66.8 ± 17.4	
Male gender (%)	1/8 (12.5%)	
Right eye (%)		
PVD	7/8 (87.5%)	
No PVD	1/8 (12.5%)	
FAZ (mm^2)		0.779
PVD	0.234 ± 0.141	
No PVD	0.282 ± 0.124	
Pseudophakic		
PVD	1/8 (12.5%)	
No PVD	2/8 (25%)	
Visual acuity (LogMAR)		0.232
PVD	0.24 ± 0.26	
No PVD	0.32 ± 0.22	
Grader 1		
Mean no. of dots		0.528
PVD	33.5 ± 47.1	
No PVD	23.3 ± 18.6	
Range of no. of dots		
PVD	3–144	
No PVD	0–64	
Mean area of largest dot (μm^2)		0.553
PVD	1660 ± 2280	
No PVD	1370 ± 1470	
Mean dot area (μm^2)		0.612
PVD	236 ± 150	
No PVD	242 ± 162	
Mean dot length (μm)		
PVD	16 ± 6	
No PVD	15 ± 8	
Grader 2		
Mean no. of dots		0.889
PVD	38.9 ± 49.8	
No PVD	31.5 ± 16.8	
Range of no. of dots		
PVD	1–151	
No PVD	12–69	
Mean area of largest dot (μm^2)		0.635
PVD	1706 ± 2479	
No PVD	1600 ± 1570	
Mean dot area (μm^2)		0.674
PVD	320 ± 303	
No PVD	263 ± 161	
Mean dot length (μm)		
PVD	19 ± 8	
No PVD	18 ± 6	

using our previously developed algorithm of HRD detection and quantification in an effort to better understand the nature of these pathoanatomical findings. We also performed high-magnification en face OCT to better understand the morphology and origin of the dots.

Methods

Study Cohort

This study was approved by the Institutional Review Board of the University of California–Los Angeles and adhered to the principles of the Declaration of Helsinki. Informed consent was obtained from each patient before en face OCT imaging, because it is not considered a routine clinical tool.

This was a retrospective cross-sectional study of patients imaged with en face OCTA (Optovue, Fremont, CA, USA) at the Stein Eye Institute between 2014 and 2019 and evaluated by one of the authors (D.S.). The OCTA database and electronic health records were queried for patients with diagnosis of epiretinal membrane (ERM), PVD, or macular hole (MH).

Inclusion criteria were OCTA examinations with a quality scan index of ≥7 for both eyes. Eyes with significant inner retinal disease or distortion caused by disorders such as lamellar macular hole, myopic foveoschisis, diabetic macular edema, or atrophy were excluded. Eyes with outer retinal disease causing significant atrophy, such as the advanced (nonneovascular or neovascular) forms of age-related macular degeneration, were also excluded. En face OCT images with significant motion artifact, segmentation errors, or degradation because of media opacity were excluded. For patients with ERM or MH, inclusion criteria were one eye status-post ILM peeling for either idiopathic MH or macular pucker and the fellow eye without ILM peeling. For patients with PVD, inclusion criteria were one eye with foveal vitreous detachment (i.e., grade 3 or 4 PVD) and one eye without foveal vitreous detachment (i.e., grade 0, 1, or 2 PVD). Patients were excluded if fellow eyes in either group harbored inner retinal changes that would confound analysis.

Imaging Protocol and Segmentation

En face OCT images were captured with a spectral-domain OCT machine (RTVue XR Avanti; Optovue, Fremont, CA, USA) and analyzed and segmented on AngioVue software Version 2017.1.0.151 (Optovue). Evaluation for foveal vitreous detachment was performed on the 6 × 6–mm scanning protocol, because recent studies suggest high accuracy using this technique.[10,11] En face OCT and OCTA images were otherwise analyzed on 3 × 3 scanning protocol only.

A method for isolating the HRD on en face OCT was previously described.[5] The structural en face OCT using the default software "superficial" slab segmentation was isolated and exported. This slab was segmented by default along the superficial vascular complex (SVC). The inner boundary of the slab was positioned 0 μm beneath the ILM, and the outer boundary was positioned 9 μm beneath the inner plexiform layer (IPL). These boundaries corresponded to the foveolar pit where there is an absence of inner layers.[12] This segmentation was chosen to reduce the foveal light reflex with en face OCT, which can mask structural HRD. Any errors in ILM automatic segmentation were manually corrected on a foveal B-scan and propagated to other cross-sections.

Multicolor confocal scanning laser ophthalmoscopy (SLO) images were captured with the Heidelberg Retinal Angiograph 2 Spectralis (Heidelberg Engineering GmbH, Heidelberg, Germany). The Heidelberg Retinal Angiograph 2 uses blue (488 nm), green (514 nm), and near-infrared (815 nm) lasers for image registration.

Quantification of Hyperreflective Dots

Two methods for quantifying HRD have been previously described.[5] Strong statistical correlation between the strategies has been validated.[5] One of the methods, a "threshold reflectivity" method of detecting and quantifying HRD, has been described in detail and was used in this study (see below). The other method involves manually counting

Investigative Ophthalmology & Visual Science

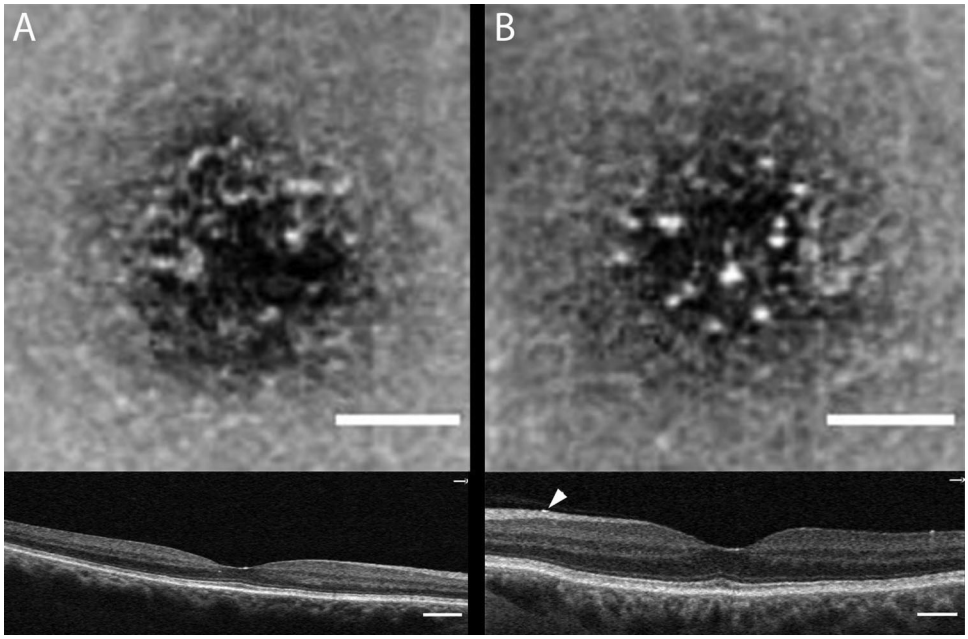

Figure 1. En face OCT with superficial segmentation and registered OCT B-scans comparing HRD in an eye with foveal PVD versus the fellow eye without foveal PVD. (**A**) *Top*: En face OCT of the right eye illustrates HRD in the fovea. *Bottom*: 6 × 6–mm OCT B scan illustrates a complete (grade 4) foveal PVD. (**B**) *Top*: En face OCT of the left eye shows HRD in the fovea. *Bottom*: 6 × 6–mm OCT B scan shows vitreous attachment with only nasal vitreous separation (*white arrowhead*) and a non-foveal grade 1 PVD. *Scale bar*: 250 µm.

the dots on the individual B-scans. Because both methods have been validated and shown to have excellent correlation, the manual counting method was deferred in this study because it cannot measure the foveal area over which the dots are localized. Two non-masked graders (C.P. and A.A.) performed the HRD analysis with the threshold reflectivity method. Briefly, using ImageJ software (1.52; http://imagej.nih.gov/ij/; provided in the public domain by the National Institutes of Health, Bethesda, MD, USA),[13] the 3 × 3–mm en face OCT image was isolated according to the borders of the foveal avascular zone (FAZ), which was determined by manufacturer's default settings, and adjusted so that all parts of this area were within the foveal depression to exclude signal from inner retinal layers. This selection was then binarized and thresholded on the basis of the mean reflectivity of the B-scan ellipsoid zone (EZ).[5] The HRD on the thresholded image could then be counted and the area measured using the ImageJ software. Given the limited resolution of OCT, it was not possible to accurately measure linear dimensions of the HRD. Therefore, to determine diameter, the polygonal dots were assumed to be approximately circular, and the software measured areas were converted to diameters (D) via the equation $D = \sqrt{\frac{area}{\pi}} * 2$.

The FAZ area may be artificially minified in patients with axial myopia, and the true FAZ is larger after correction with the manufacturer software, particularly in those with axial length >26 mm or spherical equivalent of −6 or less.[14] Axial lengths were not available for the patients in this study. Given that fellow eyes were compared and none exhibited anisometropic amblyopia, the difference in axial lengths between eyes was assumed to be insignificant, and therefore no correction factor was considered.

Since the FAZ in eyes with macular puckers both before and after surgery may be smaller,[15] the number of HRD in these eyes may be artefactually low due to the smaller area in which the HRD are measured. To offset this for the fellow eye, a correction factor of the FAZ area in the ILM peeled eye (FAZ_{ILM}) divided by the FAZ area in the fellow eye (FAZ_{FEL}), multiplied by the number of HRD (HRD_{FEL}) in the fellow eye, was used to calculate the adjusted number of fellow HRD (HRD_{adj}), also denoted by $HRD_{ADJ} = (\frac{FAZ_{ILM}}{FAZ_{FEL}} * HRD_{FEL})$.

Statistical Evaluation

All statistical analyses were performed using either Microsoft Office Excel 2016 (Microsoft Corporation, Redmond, VA, USA) or StataIC 15 (StataCorp LLC, College Station, Texas, USA). Continuous variable data were expressed as mean ± standard deviation when applicable. The Wilcoxon signed-rank test was used to compare HRD data between the groups of study eyes and fellow (control) eyes. Both the Spearman's rank correlation (ρ) and two-way mixed effect intraclass correlation coefficients were calculated to measure the agreement between graders for HRD measurements, with a confidence interval of 95%. A P value < 0.05 was considered statistically significant.

Results

Demographic and HRD data from both graders for the PVD cohort are listed in Table 1. In the PVD analysis, eight patients (one male) meeting the above inclusion and exclusion criteria were identified. The average age was 66.8 ± 17.4 years (range, 31 to 87). Seven of eight (87.5%) PVD eyes were right eyes, and of all eyes 3/16 (19%) were pseudophakic at the time of imaging. The average FAZ area was 0.234 ± 0.141 and 0.282 ± 0.124 mm^2 for the PVD and no PVD eyes, respectively ($P = 0.779$). For

Investigative Ophthalmology & Visual Science

Table 2. Comparison of Hyperreflective Dots Between Eyes With Eyes With ILM Peeling and Fellow Eyes Without ILM Peeling

		***P* Values**
ILM peel comparison		
Mean age (years)	71.2 ± 12.1	
Male gender (%)	6/10 (60%)	
Right eye (%)		
Peel	4/10 (40%)	
No peel	6/10 (60%)	
FAZ (mm^2)		0.005
Peel	0.113 ± 0.085	
No peel	0.243 ± 0.086	
Pseudophakic		
Peel	4/10 (40%)	
No peel	8/10 (80%)	
Visual acuity (LogMAR)		0.031
Peel	0.2 ± 0.13	
No peel	0.07 ± 0.09	
Grader 1		
Mean no. of dots		0.012
Peel	2.3 ± 3.0	
No peel	20.4 ± 16.7	
Mean adjusted no. of dots		0.028[a]
Peel	NA	
No peel	8.3 ±7.3	
Range of number of dots		
Peel	0–9	
No peel	1–57	
Mean area of largest dot (μm^2)		0.463
Peel	949 ± 1074	
No peel	1130 ± 1405	
Mean dot area (μm^2)		0.916
Peel	403 ± 389	
No peel	272 ± 162	
Mean dot length (μm)		
Peel	21 ± 10	
No peel	18 ± 5	
Grader 2		
Mean no. of dots		0.013
Peel	3.8 ± 4.2	
No peel	21.9 ± 16.2	
Mean adjusted no. of dots		0.037*
Peel	NA	
No peel	9.1 ± 7.4	
Range of number of dots		
Peel	0–10	
No peel	1–56	
Mean area of largest dot (μm)		0.753
Peel	1008 ± 810	
No peel	1380 ± 1995	
Mean dot area (μm^2)		0.6
Peel	323 ± 349	
No peel	310 ± 222	
Mean dot length (μm)		
Peel	20 ± 9	
No peel	19 ± 6	

* *P* value of the difference between mean no. of dots in the peeled eyes versus mean adjusted no. of dots in the fellow eyes.

Grader 1, the average number of HRD was not significantly different: 33.5 ± 47.1 (range, 0 to 151) and 23.3 ± 18.6 (range, 1 to 64) for the PVD and no PVD eyes, respectively ($P = 0.528$) (Fig. 1). Average dot area was 236 μm^2 ± 150 μm^2 and 242 μm^2 ± 162 μm^2 for the PVD and no PVD eyes, respectively ($P = 0.612$). Spearman's rhos between graders for number of HRD, average HRD area, and largest HRD were 0.87 ± 0.04, 0.84 ± 0.12, and 0.88 ± 0.10, respectively, and the intraclass correlation coefficient (ICC) for the number of HRD was 0.987 ± 0.02. The HRD were an average length of 16 ± 6 μm (range, 6 to 94 μm) in the PVD eyes, and an average length of 15 ± 8 μm (range, 6 to 72 μm) in the no PVD eyes. There was no significant difference in visual acuity between groups, with average LogMAR 0.24 ± 0.26 (Snellen equivalent 20/32) in the PVD group and 0.32 ± 0.22 in no PVD group (Snellen equivalent 20/40) ($P = 0.232$)

Demographic and HRD data from both graders for the ILM peel cohort are listed in Table 2. Ten patients (six male) meeting the above inclusion and exclusion criteria were identified. The average age was 71.2 ± 12.1 years (range, 48 to 92). Four of 10 (40%) ILM peeled eyes were right eyes, and of all eyes 12 of 20 (19%) were pseudophakic at the time of imaging. Preoperative diagnosis was ERM for six eyes and MH for four eyes. The average FAZ area was 0.113 ± 0.085 and 0.243 ± 0.086 mm^2 for the ILM peeled and fellow eyes, respectively ($P = 0.005$). For Grader 1, the average number of HRD was significantly different between groups, at 2.3 ± 3.0 (range, 0 to 10) and 20.4 ± 16.7 (range, 1 to 56) for the ILM peeled and fellow nonoperated eyes, respectively ($P = 0.012$) (Fig. 2). After applying the aforementioned FAZ correction factor to the fellow eyes, the average number of HRD was 8.3 ± 7.3, still significantly more than the ILM peeled eyes ($P = 0.028$). Average dot area was 403 μm^2 ± 389 μm^2 and 270 μm^2 ± 162 μm^2 for the ILM peeled and fellow eyes, respectively ($P = 0.916$). Spearman's rhos between graders for number of HRD, average HRD area, and largest HRD were 0.97 ± 0.03, 0.77 ± 0.14, and 0.59 ± 0.24, respectively, and the intraclass correlation coefficient for the number of HRD was 0.989 ± 0.02. The HRD were an average length of 21 ± 10 μm (range, 6 to 61 μm) in the ILM peeled eyes, and an average of 18 ± 5 μm (range, 6 to 80 μm) in the fellow eyes. There was a significant difference in visual acuity between groups, with average LogMAR 0.2 ± 0.13 (Snellen equivalent 20/32) in the ILM peeled group and 0.07 ± 0.09 (Snellen equivalent 20/25) in fellow eye group ($P = 0.031$)

Multicolor confocal SLO imaging was available in four patients in the PVD cohort and four patients in the ILM peeled cohort. Qualitatively, the HRD appeared less numerous and bright (Fig. 3) than noted previously with SLO imaging.[1,16] The HRD were best identified with either green or blue reflectance but could not be detected with near-infrared. Additionally, the HRD appeared less numerous and less distinct when compared with en face OCT.

Higher-magnification en face OCT imaging was performed in all cases that had at least 10 HRD on counts by both graders. Nineteen of the 36 total eyes displayed at least 10 HRD, and 13 of those 19 displayed HRD demonstrating an irregular polygonal shape with fine ciliary-like or dendriform extensions (Fig. 4).

Discussion

Corradetti et al.[5] were the first to identify superficial hyperreflective dots in the central fovea of normal eyes using en face OCT and showed a systematic increase according to age. In this study, we attempted to better understand the morphology and origin of these lesions and the effect of PVD and ILM peeling. Although there were no significant differences in the number of HRD in the eyes with foveal

Investigative Ophthalmology & Visual Science

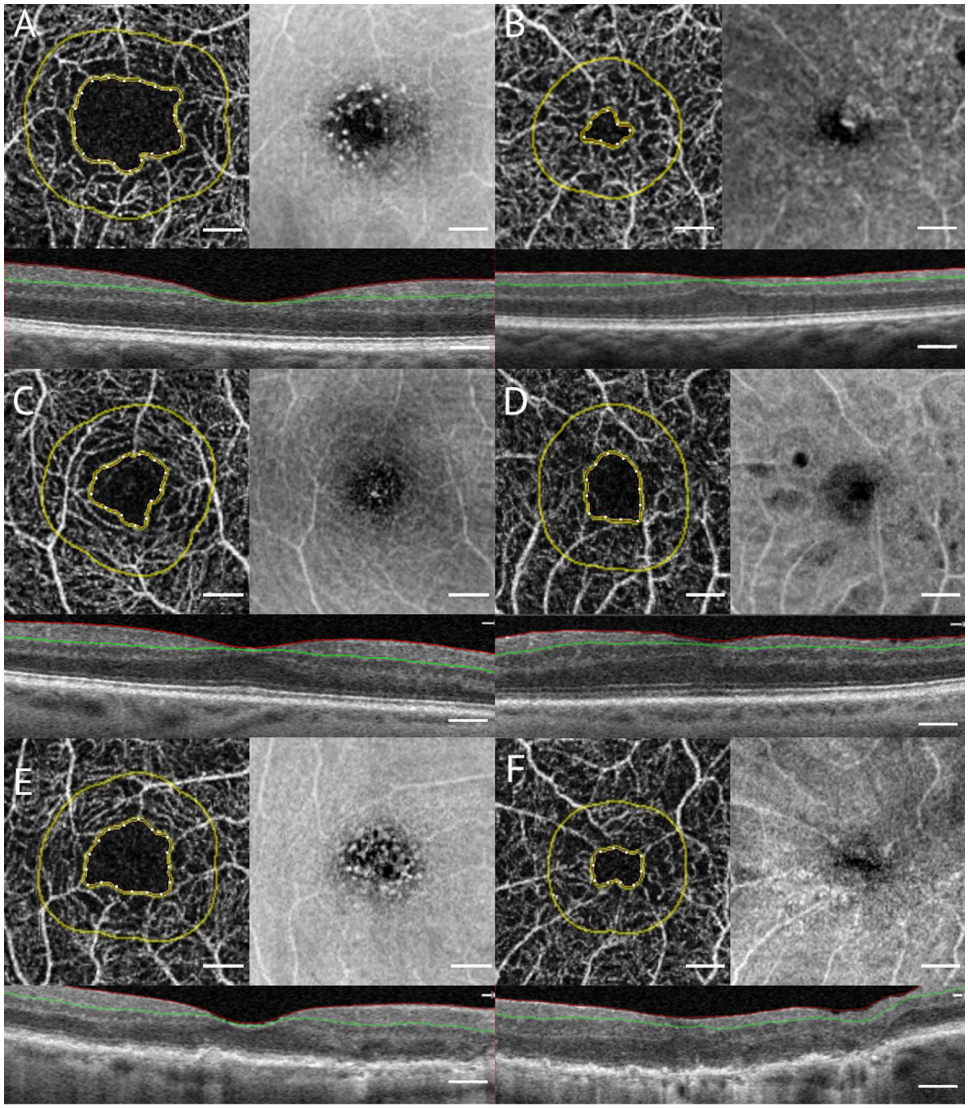

Figure 2. En face OCT angiography and structural en face OCT with superficial segmentation and registered OCT B-scans comparing HRD in three nonoperated fellow eyes (**A, C, E**) versus three eyes after ILM peeling (**B, D, F**). Note the presence of multiple HRD in the central fovea of the ILM peel eyes (**B, D, F**) and the virtual absence of HRD in the nonoperated fellow control eyes (**A, C, E**). Foveal avascular zone is smaller in the operated eyes, but an algorithm was used to compensate for this discrepancy. *Scale bar*: 250 µm.

PVD versus eyes with earlier grades of PVD without foveal detachment, the number of dots was greater in the former group.

This study also studied eyes with ILM peeling for macular hole surgery and found that there was a significant reduction in the number of HRD in the eyes with ILM peel versus the fellow nonoperated eyes, even after adjusting for decreased FAZ area. Corradetti et al were not able to determine the exact nature of these HRD and speculated that the lesions could represent Muller cell endfeet versus ILM processes versus vitreous hyalocytes. The greater number of HRD with age in the Corradetti study and the reduced number after ILM peel in this study indicates that vitreous hyalocytes are very unlikely to represent the HRD.

It is still unclear whether the HRD represent acellular material, such as collagen or extracellular matrix, or nucleated cells with processes. However, magnification of the en face OCT images illustrated that the HRD displayed irregular shapes with fine ciliary-like or dendriform extensions along the retinal surface. Yokotsuka et al.,[1] in their seminal study, described the white dot fovea. Their landmark SEM illustrations displayed "ciliary-like" extensions associated with the white dots that were remarkably similar to the magnified en face images of the HRD illustrated in our study (Fig. 4). These granules were polygonal, measured between 5 µm and 20 µm in length, were comprised of multiple processes and cilia-like extensions, and were scattered diffusely over the foveal surface, findings that remarkably correspond to the findings in this study and in the study of Corredetti et al.[5] Moreover, in studies of ILM tissue after macular hole[17] or ERM[18] surgery in humans, a population of epiretinal cells with irregular short processes and hair-like cell extensions was found on SEM, similar to those shown by Yokotsuka et al.[1] Yokotsuka et al.[1] also displayed the white dots clinically with SLO. In this study, we were also able to show that the en face OCT HRD could be identified with SLO, especially with the green channel. It is unclear

Investigative Ophthalmology & Visual Science

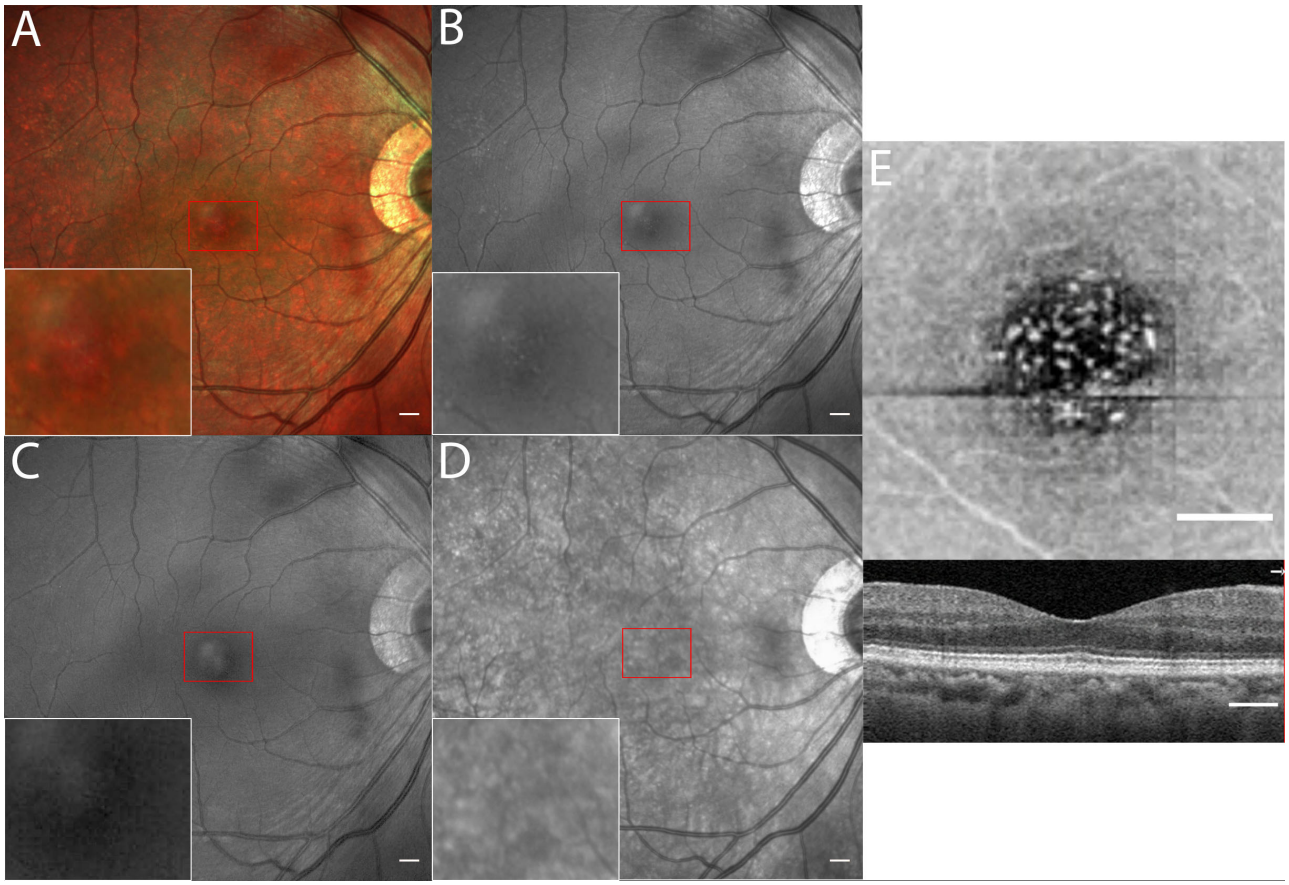

Figure 3. Montage of a right eye with PVD. SLO images including multicolor (**A**), green (**B**), blue (**C**), and near-infrared (**D**) demonstrate characteristic HRD most notable on green channel, although they are more prominent with en face OCT (E). *Scale bars* for **A, B, C, D**: 500 µm. *Scale bar* for **E**: 250 µm.

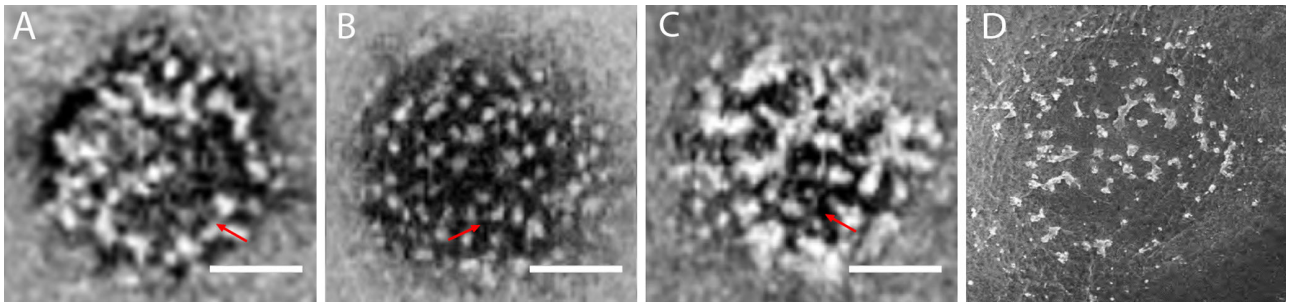

Figure 4. High-magnification en face OCT images with superficial segmentation of three eyes with HRD. (**A**) A left eye with no PVD from an 87-year-old female. (**B**) A right eye, fellow eye of ILM-peeled eye from a 73-year-old female. (**C**) A right eye, fellow eye of ILM-peeled eye, from a 92-year-old female. (**D**) The scanning electron microscopy image borrowed from Yokotsuka et al.[1] (Reprinted from American Journal of Ophthalmology, Volume 123, Yokotsuka et al, White Dot Fovea, Pages 76–83, 1997, with permission from Elsevier). Note the polygonal HRD with fine dendritic or cilia-like extensions that extend from the HRD, suggestive of activated cell processes (*red arrows*). *Scale bar*: 250 µm.

why HRD were move visible with the green channel versus the blue channel. This may be due to absorption properties of the HRD or wavelength interactions with macular pigment.[19] Therefore it is very likely that the en face OCT HRD described in this study, and in the Corradetti study, represent the white dot fovea described by Yokotsuka et al.[1] using SEM. Note that subsequent publications of white dot fovea[16,20] illustrated more pathological features suggestive of macular disease and likely do not represent the anatomical landmarks described in the article by Yokotsuka et al.[1] and in our studies.

Furthermore, the ILM is known to be especially thin in the fovea[21] and around vessels.[22] The fovea represents an anatomical location of increased vitreoretinal traction.[23] Foos[24] originally hypothesized that PVD-induced ILM microbreaks facilitated the extension of glial cells along the

Investigative Ophthalmology & Visual Science

retinal surface. These glia were thought to act as the scaffold for later ERM formation. Similarly, in other areas of increased vitreoretinal traction, such as around the retinal vasculature, activated Muller cells can break through the ILM and grow along the surface of the retina.[22,25] Both EM[23,24] and immunohistochemical[26] studies have demonstrated this population of Muller and glial cells most prominently in areas of ILM thinning. These characteristic cells have been referred to as epivascular glia and exhibit similar glial characteristics of cilia-like or dendritic extensions consistent with the HRD described in this study in the fovea. Our group has recently identified and described epivascular glia, that are most prominent around the major temporal vessels with en face OCT, and these lesions have similar morphological characteristics to the HRD including the cilia-like or dendriform processes.[27]

The lack of difference of HRD numbers with PVD in this study suggest that the force generated during foveal vitreous separation is insufficient to avulse the HRD, the HRD grow back after PVD, or these HRD integrate at a deeper layer that may be removed during ILM peeling. Spontaneous PVD tends to progress slowly in a stepwise fashion,[28] and recent observations suggest that the posterior hyaloid face is formed as a split from the ILM during PVD.[29] Chronic vitreoretinal traction preceding PVD may stimulate anterior migration such as occurs around the retinal vasculature. It is possible that HRD therefore may represent glial or Muller cell protrusions through the thin ILM caused by vitreoretinal traction or detachment. Although we did not identify a significant difference in the number of HRD in eyes with foveolar detachment, the number was still greater in this group. Microtrauma to the ILM may induce glial activation, in which cellular processes plug these defects. With larger defects, whole nucleated cells may migrate onto the retinal surface, similar to the process described with lamellar hole epiretinal proliferations.[30] With a much larger recruitment of eyes, a significant difference may be elicited.

Limitations of this study include the retrospective nature of the analysis and the small sample size in both groups. The cross-sectional methodology of this study should be validated with longitudinal analysis. During idiopathic MH formation, an inner foveal cap of varying thickness may be avulsed,[25] so we are unable to determine whether the loss of HRD results from ILM peeling or MH pathogenesis. However, we found no difference between the number of HRD in ILM peeled eyes with ERM versus MH, although the number for each group was small, and larger groups may show a difference. Outer retinal changes such as age-related macular degeneration in some eyes may have introduced error, but changes were bilateral, symmetric, and with no notable inner retinal effects. The small angles of tilt of the B-scan that introduce artifacts in the Henle fiber layer may affect imaging of the HRD,[31] but given the planar configuration of the HRD across the superficial retina, the effect is likely minimal. Comparison of preoperative and postoperative HRD analysis would be ideal, but limitations of available segmentation algorithms on OCT devices prevents accurate preoperative en face segmentation of the superficial layers caused by ERM wrinkling, retinal thickening, or layer disorganization. Additionally, the absence of foveal tissue with macular holes precludes assessment of HRD.

In conclusion, ILM peeled eyes displayed a decreased number of HRD with en face OCT imaging compared with fellow eyes, although additional data is needed to fully evaluate the effect of a PVD. These HRD exhibit a size (15 to 20 um) and morphology with cilia-like extensions closely resembling the white dot fovea described decades ago with scanning electron microscopy,[1] and therefore these dots may represent processes of activated glial cells, possibly Muller cells, traversing defects in the ILM. Further imaging and clinicopathological inquiries examining other inner foveal disorders may prove informative in elucidating the structure and function of these dots.

Acknowledgments

Disclosure: **C. Pole,** none; **A. Au,** None; **E. Navajas,** None; **K.B. Freund,** HealthCare/Regeneron (F, C), Roche/Genentech (F, C), Heidelberg Engineering (C), Novartis (C), Allergan (C), Carl Zeiss Meditec (C); **S. Sadda,** Optos (F, C), Centervue (F, C), Heidelberg (F, C), Nidek (C), Topcon (C), Carl Zeiss Meditec (C); **D. Sarraf,** Heidelberg Engineering (F), Optovue (F, I, C), Topcon (F)

References

1. Yokotsuka K-I, Kishi S, Shimizu K. White dot fovea. *Am J Ophthalmol*. 1997;123:76–83.
2. Fujimoto J, Swanson E. The development, commercialization, and impact of optical coherence tomography. *Invest Ophthalmol Vis Sci*. 2016;57(9):OCT1–OCT13.
3. Keane PA, Sadda SR. Retinal imaging in the twenty-first century: state of the art and future directions. *Ophthalmology*. 2014;121:2489–2500.
4. Hirano M, Morizane Y, Kimura S, et al. Assessment of lamellar macular hole and macular pseudohole with a combination of en face and radial B-scan optical coherence tomography imaging. *Am J Ophthalmol*. 2018;188:29–40.
5. Corradetti G, Au A, Borrelli E, Xu X, Freund KB, Sarraf D. Analysis of hyperreflective dots within the central fovea in healthy eyes using en face optical coherence tomography. *Invest Ophthalmol Vis Sci*. 2019;60:4451–4461.
6. Ghasemi Falavarjani K, Phasukkijwatana N, Freund KB, et al. En face optical coherence tomography analysis to assess the spectrum of perivenular ischemia and paracentral acute middle maculopathy in retinal vein occlusion. *Am J Ophthalmol*. 2017;177:131–138.
7. Clamp MF, Wilkes G, Leis LS, et al. En face spectral domain optical coherence tomography analysis of lamellar macular holes. *Retina Phila Pa*. 2014;34:1360–1366.
8. Ahn SJ, Joung J, Lee BR. En face optical coherence tomography imaging of the photoreceptor layers in hydroxychloroquine retinopathy. *Am J Ophthalmol*. 2019;199:71–81.
9. Thulliez M, Motulsky EH, Feuer W, Gregori G, Rosenfeld PJ. En face imaging of geographic atrophy using different swept-source OCT scan patterns. *Ophthalmol Retina*. 2019;3:122–132.
10. Kraker JA, Kim JE, Koller EC, George JC, Hwang ES. Standard 6 mm compared to wide field 16.5 mm optical coherence tomography for staging of posterior vitreous detachment. *Ophthalmol Retina*. 2020;4:1093–1102.
11. Hwang ES, Kraker JA, Griffin KJ, Sebag J, Weinberg DV, Kim JE. Accuracy of spectral-domain OCT of the macula for detection of complete posterior vitreous detachment. *Ophthalmol Retina*. 2020;4:148–153.
12. Syrbe S, Kuhrt H, Gärtner U, et al. Müller glial cells of the primate foveola: an electron microscopical study. *Exp Eye Res*. 2018;167:110–117.
13. Schneider CA, Rasband WS, Eliceiri KW. NIH Image to ImageJ: 25 years of image analysis. *Nat Methods*. 2012;9:671–675.

14. Suda M, Yoshikawa Y, Terauchi G, et al. Magnification effect of foveal avascular zone measurement using optical coherence tomography angiography. *Biomed Hub*. 2020;5(2): 1–8.
15. Kitagawa Y, Shimada H, Shinojima A, Nakashizuka H. Foveal avascular zone area analysis using optical coherence tomography angiography before and after idiopathic epiretinal membrane surgery. *RETINA*. 2019;39:339–346.
16. Witkin AJ, London NJS, Wender JD, Fu A, Garg SJ, Regillo CD. Spectral-domain optical coherence tomography of white dot fovea. *Arch Ophthalmol*. 2012;130:1603–1605.
17. Schumann RG, Eibl KH, Zhao F, et al. Immunocytochemical and ultrastructural evidence of glial cells and hyalocytes in internal limiting membrane specimens of idiopathic macular holes. *Invest Ophthalmol Vis Sci*. 2011;52:7822–7834.
18. Schumann RG, Gandorfer A, Ziada J, et al. Hyalocytes in idiopathic epiretinal membranes: a correlative light and electron microscopic study. *Graefes Arch Clin Exp Ophthalmol*. 2014;252:1887–1894.
19. Feng HL, Sharma S, Stinnett S, Asrani S, Mruthyunjaya P. Identification of posterior segment pathology with en face retinal imaging using multicolor confocal scanning laser ophthalmoscopy. *RETINA*. 2019;39:972–979.
20. Fekrat S, Humayun MS. White dot fovea in an African American patient. *Arch Ophthalmol*. 1998;116:110–111.
21. Sebag J. Age-related differences in the human vitreoretinal interface. *Arch Ophthalmol*. 1991;109:966–971.
22. Kishi S, Numaga T, Yoneya S, Yamazaki S. Epivascular glia and paravascular holes in normal human retina. *Graefes Arch Clin Exp Ophthalmol*. 1986;224:124–130.
23. Foos RY. Vitreoretinal juncture over retinal vessels. *Graefes Arch Clin Exp Ophthalmol*. 1977;204:223–234.
24. Foos RY. Vitreoretinal juncture; epiretinal membranes and vitreous. *Invest Ophthalmol Vis Sci*. 1977;16:416–422.
25. Gaudric A, Haouchine B, Massin P, Paques M, Blain P, Erginay A. Macular hole formation: new data provided by optical coherence tomography. *Arch Ophthalmol Chic Ill 1960*. 1999;117:744–751.
26. Edwards MM, McLeod DS, Bhutto IA, Villalonga MB, Seddon JM, Lutty GA. Idiopathic preretinal glia in aging and age-related macular degeneration. *Exp Eye Res*. 2016;150:44–61.
27. Grondin C, Au A, Wang D, et al. Identification and characterization of epivascular glia using en face OCT. *Am J Ophthalmol*. 2021;229:108–119.
28. Johnson MW. Posterior vitreous detachment: evolution and complications of its early stages. *Am J Ophthalmol*. 2010;149:371–382.e1.
29. Fincham GS, James S, Spickett C, et al. Posterior vitreous detachment and the posterior hyaloid membrane. *Ophthalmology*. 2018;125:227–236.
30. Pang CE, Maberley DA, Freund KB, et al. Lamellar hole–associated epiretinal proliferation: a clinicopathologic correlation. *RETINA*. 2016;36:1408–1412.
31. Lujan BJ, Roorda A, Knighton RW, Carroll J. Revealing Henle's fiber layer using spectral domain optical coherence tomography. *Invest Ophthalmol Vis Sci*. 2011;52:1486–1492.

Investigative Ophthalmology & Visual Science